DOI 10.59887/2073-6673.2025.18(2)-11

EDN QWDKNG

УДК 551.46.08

© *V. A. Glukhov**, *Yu. A. Goldin*, *O. V. Glitko*, 2025
© Translation from Russian: *V.A. Glukhov*, 2025
Shirshov Institute of Oceanology, Russian Academy of Sciences, 36 Nakhimovsky Prosp., Moscow 117997, Russia
*E-mail: vl.glukhov@inbox.ru

Investigation of the Dependence of Lidar Echo Signal Characteristics on the Length of the Sounding Path

Received 23.04.2025, Revised 14.06.2025, Accepted 20.06.2025

Abstract

Field measurements of the characteristics of the bottom-reflected lidar echo signal were conducted in the waters of Bechevinskaya Bay. The studies employed the APL-3 airborne polarization lidar (sounding pulse energy of 45 mJ, receiving optical system diameter of 100 mm, and system response function duration at the 0.5 level of 10.8 ns). The depth range during the investigations varied from 3 to 22 m, while the flight altitude ranged from 500 to 1200 m. The hydrooptical characteristics of the bay waters were assessed based on lidar sounding data. For the analysis of field measurement data, areas with similar values of the lidar attenuation coefficient were selected. The results of field experiments demonstrated that the relationship between the magnitude of the lidar echo signal and the length of the sounding path for water layers and the seabed is more complex than what is suggested by the conventional form of the lidar equation. The introduction of an additional term into the lidar equation, which defines the dispersion of the irradiance distribution in the cross-section of an infinitely narrow beam of light passing through a water layer of a given thickness, allowed for a more accurate description of the obtained experimental dependencies. The registered effect must be taken into account when designing lidar systems, as well as during the processing and analysis of lidar survey data.

Keywords: bathymetric lidar, bathymetric survey, lidar equation, sounding altitude, geometric factor

© *В. А. Глухов**, *Ю. А. Гольдин*, *О. В. Глитко*, 2025
© Перевод с русского: *В.А. Глухов*, 2025
Институт океанологии им. П.П. Ширшова РАН, 117997, г. Москва, Нахимовский пр., д. 36
*vl.glukhov@inbox.ru

Исследование зависимости характеристик лидарного эхо-сигнала от протяженности трассы зондирования

Статья поступила в редакцию 23.04.2025, после доработки 14.06.2025, принята в печать 20.06.2025

Аннотация

Натурные измерения характеристик отраженного от дна эхо-сигнала выполнены в акватории Бечевинской бухты. При проведении исследований использован авиационный поляризационный лидар АПЛ-3 (энергия зондирующего импульса 45 мДж, диаметр приемной оптической системы 100 мм, длительность импульсной характеристики лидара по уровню 0,5–10,8 нс). Диапазон изменения глубин при проведении исследований составил от 3 до 22 м, высота полета менялась от 500 до 1200 м. Оценка гидрооптических характеристик вод бухты проводилась по данным лидарного зондирования. Результаты натурных экспериментов показали, что зависимость величины и формы лидарного эхо-сигнала от протяженности трассы зондирования при регистрации слоев воды

Ссылка для цитирования: *Глухов В.А.*, *Гольдин Ю.А.*, *Глитко О.В.* Исследование зависимости характеристик лидарного эхо-сигнала от протяженности трассы зондирования // Фундаментальная и прикладная гидрофизика. 2025. Т. 18, № 2. С. 151–161. https://doi.org/10.59887/2073-6673.2025.18(2)-11 EDN QWDKNG
For citation: Glukhov V.A., Goldin Yu.A., Glitko O.V. Investigation of the Dependence of Lidar Echo Signal Characteristics on the Length of the Sounding Path. *Fundamental and Applied Hydrophysics*. 2025;18(2):151–161.
https://doi.org/10.59887/2073-6673.2025.18(2)-11

и морского дна имеет более сложный вид, чем это следует из общепринятой формы записи лидарного уравнения. Введение дополнительного члена в лидарное уравнение, определяющего дисперсию распределения освещенности в поперечном сечении бесконечно узкого пучка света, прошедшего через водный слой заданной толщины, позволило более точно описать полученные экспериментальные зависимости. Зарегистрированный эффект необходимо учитывать при проектировании лидарных комплексов, а также при обработке и анализе данных лидарной съемки.

Ключевые слова: батиметрический лидар, батиметрическая съемка, лидарное уравнение, высота зондирования, геометрический фактор

1. Introduction

Marine profiling (radiometric) lidars enable the solution of a number of oceanographic problems [1–3]. Among them, we can highlight the registration of the positions of light scattering layers [4, 5], the determination of hydrooptical characteristics of the near-surface layer of seawater and their spatial variability [6–9], as well as the observation of internal waves [10–12]. A special focus is placed on laser bathymetry [13]. This is the most developed area of lidar remote sensing. Several lidar bathymetric systems are known, designed as certified measuring instruments [14–16]. Such systems are used to register the variability of the sea floor depth in shallow coastal sea areas, to monitor the condition of navigation channels, and for studying the bottoms of inland water bodies and rivers [16, 17].

The lidar sounding path consists of atmospheric and underwater segments. Depending on the target of the sounding and the water transparency, the length of the underwater segment can range from a few meters to several tens of meters. The range of variation for the atmospheric segment is significantly greater. In underwater lidars, the atmospheric segment is absent. In shipborne lidars, its length typically varies from 1 to 20 meters. In airborne lidars, the length of the atmospheric segment can range from 50 meters to 500 meters. In certain cases, it may extend to lengths of 1 to 2 kilometers [18] and even up to approximately 10 kilometers [19]. When the lidar is placed on a satellite, the length of the atmospheric segment can increase to hundreds of kilometers [20].

Typically, in the process of lidar surveying, the altitude at which the lidar is positioned remains fixed, resulting in a lack of experimental data regarding the dependence of survey results on altitude. Nonetheless, the length of the atmospheric segment significantly affects the amplitude and shape of the lidar echo signal decay. Works [13, 21, 22] utilize an analytical solution to the transfer equation in a small-angle approximation to investigate the influence of the sounding path length on the magnitude of the echo signal reflected from the seabed. The dependencies of the echo signal amplitudes reflected from the surface, water column, and seabed on the sounding path length, derived from calculations [13, 21, 22], differ from the widely accepted inverse square law. They exhibit a more complex behavior. The aim of this study is to experimentally investigate the dependence of the amplitude and shape of the echo signals reflected from the water layers and the seabed on the lengths of the atmospheric and underwater segments of the sounding path.

2. Materials and Methods

2.1. Description of the Equipment

For the research, the airborne polarization lidar APL-3 (developed by the Shirshov Institute of Oceanology Russian Academy of Sciences [23]) was utilized. The digital four-channel oscilloscope LeCroy HDO4034 was employed for digitizing and recording the lidar echo signals. The optical unit of the lidar was mounted above the open optical window of the laboratory aircraft at an angle of $\varphi = 15°$ from the vertical, which minimized the impact of laser beam specular reflections from the disturbed water surface. During the lidar survey, the cross-polarized component of the lidar echo signal was recorded. The main technical specifications of the APL-3 lidar are summarized in Table 1.

Table 1

Main technical characteristics of the APL-3 lidar

Characteristic	Value
Wavelength of the sounding radiation, nm	532
Duration of the sounding pulse Δt, ns	7

Fin table 1

Characteristic	Value
Energy of the sounding pulse W_0, mJ	45
Sounding frequency, Hz	30
Beam divergence of the sounding pulse $2\theta_1$, mrad	5
Field of view angle of the receiving optical system of the cross-polarized channel $2\theta_2$, deg. (mrad)	2 (35)
Diameter of the input lens of the cross-polarized channel, mm	100
ADC resolution, bits	14
Digitizing frequency of lidar echo signals, GHz	2.5

2.2. Research Area

Experimental studies were conducted in August 2018 in the area of Bechevinskaya Bay in Avacha Bay on the Kamchatka Peninsula [18, 24]. The spatial configuration of the flight paths is illustrated in Fig. 1. The bay is surrounded by hills with an elevation of approximately 1 km. Safety regulations limited measurements to the entrance of the bay. During the lidar bathymetric survey, four flight paths were performed at altitudes of 500, 700, 900, and 1200 m. The seabed in the bay is characterized by varying depths, allowing for the acquisition of lidar echo signals corresponding to bottom depths ranging from 3 to 22 m over a relatively small area. During the field experiment, the state of the water surface was close to calm, with wind speeds not exceeding 2 m/s. This is corroborated by visual observations from the aircraft using a camera mounted in the photohatch.

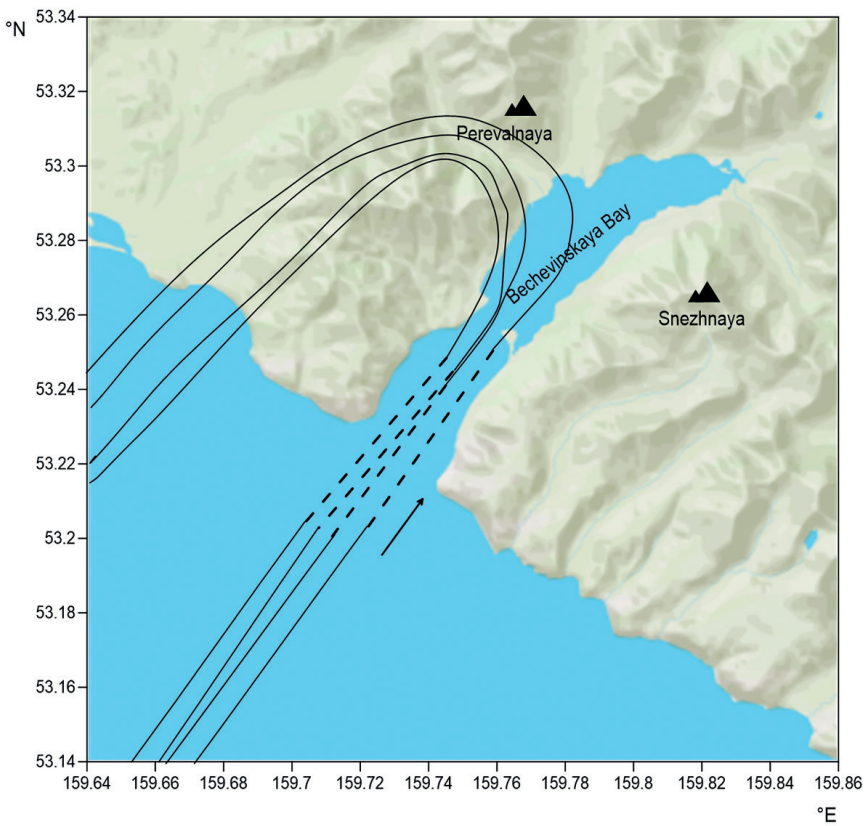

Fig. 1. Flight path over Bechevinskaya Bay. The dashed lines indicate the sections where lidar sounding was performed. The arrow shows the direction of flight along the tracks

2.3. Lidar data processing method

The processing of lidar data for seabed surveying was carried out using the standard method employed in bathymetric surveys [13, 24, 25]. An example of seabed depth determination z_b is illustrated in Fig. 2. The reference point is defined as the moment the echo signal reflected by the surface layers of water. The point of return from the seabed is considered its position. Subsequently, the time interval Δt_b between the moments of receiving pulses from the surface layers of water t_s and from the seabed t_b is calculated:

$$\Delta t_b = t_b - t_s. \tag{1}$$

The bottom depth z_b is determined by the formula:

$$z_b = \frac{c_w \Delta t_b}{2}, \tag{2}$$

where c_w is the speed of light in seawater. In the case where the bottom return signal is located on the trailing edge of the lidar echo signal, the amplitude of the bottom signal P_b is determined as the difference between the peak amplitude of the bottom return and the amplitude of the water column signal at the time corresponding to the peak of the bottom return. An example of such an echo signal, acquired from an altitude of 900 m at a bottom depth of 12.7 m, is shown in Fig. 2a. In the case where the bottom return is formed in a section where the level of the water column echo signal is below the noise floor of the receiver-recording system, its amplitude P_b is measured relative to the noise level. An example of such an echo signal, acquired from an altitude of 500 m at a bottom depth of 21.5 m, is shown in Fig. 2b.

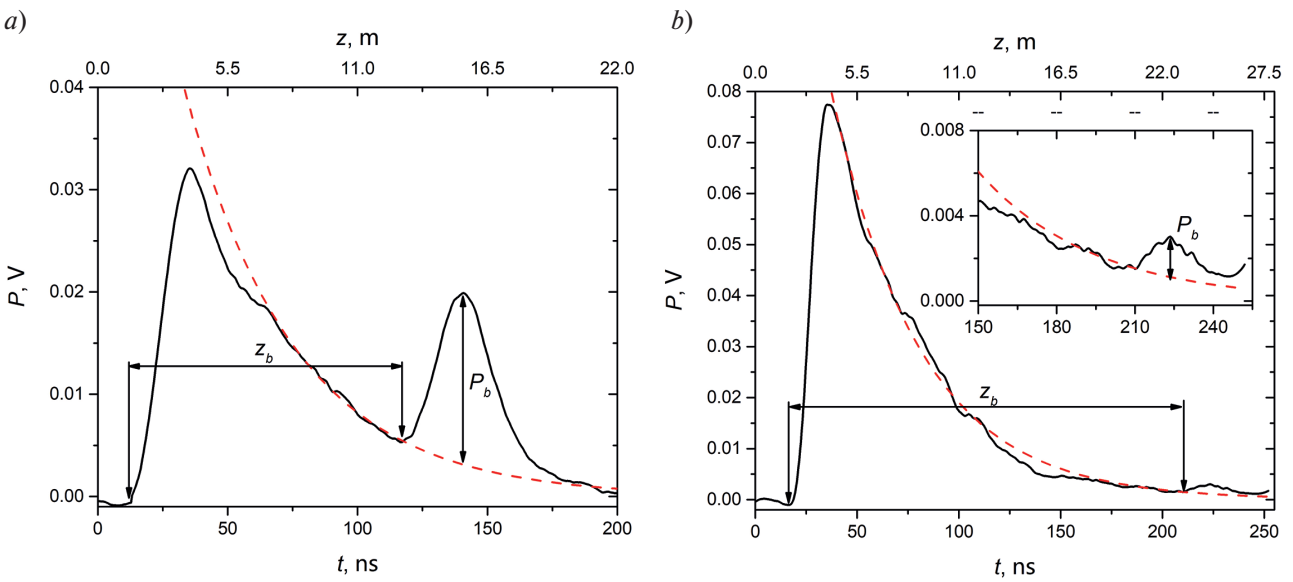

Fig. 2. Examples of lidar echo signals illustrating the method for determining the bottom depth z_b and the amplitude of the bottom signal P_b, obtained from an altitude of 900 m at a bottom depth of 12.7 m (*a*) and from an altitude of 500 m at a bottom depth of 21.5 m (*b*)

3. Results and Discussion

The power of the lidar echo signal P as a function of time t is described by the lidar equation [1, 26]. In its conventional form, the equation is expressed as follows:

$$P\left(t = \frac{2Z}{c_w}\right) = \frac{c_w W_0 A T_O (1-r)^2}{2(n_w H + Z)^2} \beta'(\pi, Z) \exp\left[-2\int_0^Z \alpha(Z')dZ'\right], \tag{3}$$

where Z and H represent the lengths of the underwater and atmospheric segments of the sounding path, respectively; c_w is the speed of light in seawater; n_w is the refractive index of seawater; W_0 is the energy of the sounding

pulse; A is the area of the receiving aperture; T_O is the transmittance of the receiving system; r is the Fresnel reflection coefficient for the air-seawater interface; $\alpha(Z)$ is the lidar attenuation coefficient; $\beta'(\pi, Z)$ is the effective value of the volume scattering function (VSF) at the scattering angle $\theta = 180°$. The true depth z can be recalculated from Z accounting for the sounding angle φ. The time t is measured from the moment when the sounding pulse crosses the water surface. When calculating the bottom-reflected echo signal, the expression $\frac{c_w \Delta t}{2} \cdot 2\pi\beta'(\pi, Z)$ is replaced with the bottom reflectance coefficient R_b. The dependence of echo signal power P on the sounding path length is determined by the so-called geometric factor $(n_w H+Z)^{-2}$.

The lidar Eq. (3) is derived under the assumption of single backscattering. It also assumes that the receiver's field-of-view angle is significantly larger than the initial laser beam divergence ($\theta_1^2 << \theta_2^2$) and sufficiently wide to capture all radiation backscattered from the corresponding water layer depth. Under field conditions, due to multiple scattering along the path from the water surface to the target and back, this assumption is not always valid. A more universal formula is required that remains applicable when the laser spot at the depth of the sounded layer does not fully fall within the photodetector's field of view. The formula satisfying this requirement takes the form [27]:

$$P(Z) = \frac{\left(c_w W_0 / 4\pi n_w^2\right) A\theta_2^2 T_0 (1-r)^2}{\theta_2^2 (H + Z/n_w)^2 + 2D(Z)} \cdot b_b(Z) \cdot \exp\left(-2\int_0^Z \alpha(z)\, dz\right), \quad (4)$$

$$D(Z) = \frac{2}{q^2}\int_0^Z b_f(z)(Z-z)^2\, dz, \quad (5)$$

where $2\theta_2$ is the photodetector's field-of-view angle; $b_b(Z) = 2\pi\beta'(\pi, Z)$ is the backscattering coefficient; $\alpha(Z) = a(Z) + 2b_b(Z)$, $a(Z)$ is the absorption coefficient; $D(Z)$ is the variance of the irradiance distribution in the cross-section of an infinitely narrow light beam after propagating through a water layer of thickness Z; $b_f(Z) = b(Z) - 2b_b(Z)$ is the forward scattering coefficient, with $b(Z)$ being the total scattering coefficient; q is the parameter of the forward section of the scattering phase function, which defined as:

$$x_f(\theta) = \frac{2q}{\theta}\exp(-q\theta). \quad (6)$$

Equation (4) was derived by computing the power of a single-backscattered pulse signal while accounting for multiple small-angle forward scattering events. This calculation employs a solution to the radiative transfer equation under the small-angle diffusion approximation as the beam spread function (BSF). Equation (4) incorporates the additional term $2D(Z)$, which quantifies the broadening of both the transmitter's and receiver's effective radiation patterns. This broadening results from multiple forward scattering during the two-way propagation of light through a water column of thickness Z. When $b_1 = \text{const}$, the function $D(Z)$ can be expressed as:

$$D(Z) = \frac{2}{3q^2} b_1 Z^3. \quad (7)$$

The array of field measurement data collected in the Bechevinskaya Bay allows for the assessment of the applicability of the lidar equation formulations using Eq. (3) and (4) for describing the backscattered signal power from the seabed and the water column at a specified depth. The experimental data were processed for seabed depths of 8 m, 10 m, 12 m, 15 m, and 17 m, recorded at altitudes of 500 m, 700 m, 900 m, and 1200 m. For each of the four altitudes, sounding points were selected for the specified depths that were spatially close and had similar values of the lidar attenuation coefficient α, which is dependent on hydrooptical characteristics. It was also assumed that the seabed reflection coefficient R_b at the selected points remains constant. The amplitude of the echo signal from the seabed P_b was determined for each sounding. The lidar data processing method for determining P_b is presented in Section 2.3. For subsequent analysis, the amplitude of the echo signal P_b was averaged over 10 successive measurements.

To evaluate the attenuation of the lidar echo signal from the depth Z_b and the length of the atmospheric segment of the sounding path H, two approximation functions were employed, the forms of which are derived from the representations of the lidar Eq. (3) and (4). For convenience, we present formulas (3) and (4) in the following form:

$$P(H,z)=\frac{f_1(z)}{f_2(H,z)}, \tag{8}$$

$$P(H,z)=\frac{f_1(z)}{f_2(H,z)+f_3(z)}, \tag{9}$$

$$f_1(z)=\frac{c_w}{4n_w^2}W_0AT_0\theta_2^2(1-r)^2b_b(z)\exp\left(-2\int_0^z\alpha(z')dz'\right), \tag{10}$$

$$f_2(H,z)=\theta_2^2\left(H+\frac{z}{n_w}\right)^2, \tag{11}$$

$$f_3(z)=\frac{2}{3q^2}b_1z^3. \tag{12}$$

For each specified depth z, the dependence of the echo signal attenuation P on the flight altitude is determined solely by the geometric factor $f_2(H, z)$. Consequently, formulas (8) and (9) can be utilized to approximate the experimental data obtained for given depths z at various sounding altitudes H. The values of functions $f_1(z)$ and $f_3(z)$ will be constants of approximation determined by the least squares method. Figure 3 presents the averaged values of the echo signal amplitudes during Fresnel reflection from the water surface P_F, as well as values of P_b for depths of 8, 12, 15, and 17 m, recorded from different sounding altitudes. The approximation of the experimental data using Eq. (8) is indicated by a blue dashed line, while the approximation using Eq. (9) is shown in red. In the case of Fresnel reflection from the water surface P_F, the approximation curves coincide; however, in other cases, they differ. It is evident that for depths greater than 8 m, the approximation curve constructed using Eq. (9) provides a better fit to the field measurement data.

Echo signal measurements were conducted for water layers at depths of 3, 8, 10, 12 and 15 m. The amplitude values of the echo signals were measured at the entrance to the bay, where the seabed depth exceeds 22 m. For different altitudes, sounding points were selected that were closely located in spatial position. Figure 4 presents the amplitude values of the echo signal for the maximum from the upper water layers P_{max}, where, for cross-polarization, the maximum occurs at a depth of approximately 3 m. Additionally, the amplitude values P for depths of 8, 12, and 15 m are also shown.

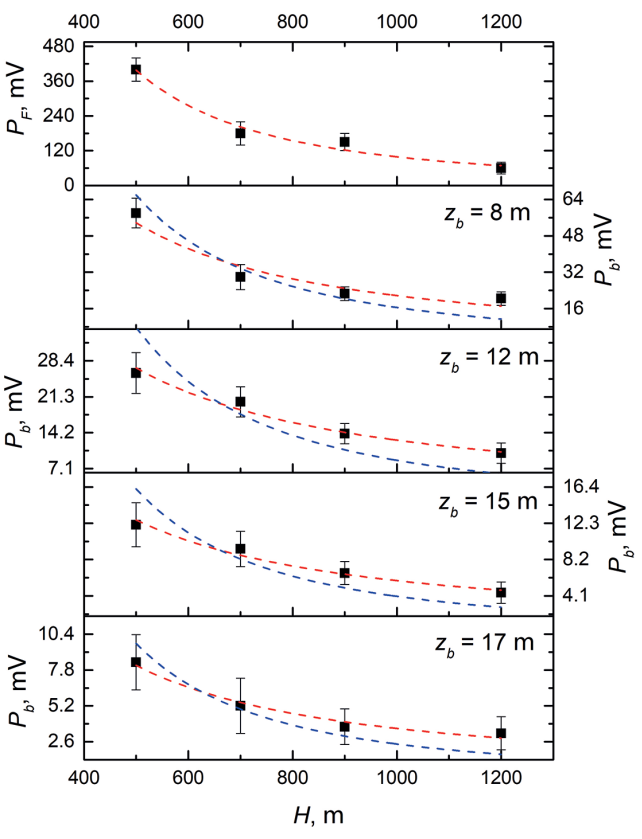

Equation (9) demonstrates that by having two recordings of the signal $P(H, z)$ as functions of depth z, obtained from closely positioned points at two different heights H_1 and H_2, it is possible to determine the function $f_3(z)$ as follows:

$$f_3(z)=\frac{f_2(H_1,z)P\left(H_1,z\right)-f_2(H_2,z)P\left(H_2,z\right)}{P\left(H_2,z\right)-P\left(H_1,z\right)}. \tag{13}$$

Fig. 3. Values of the echo signal amplitude for the case of Fresnel reflection from the water surface P_F, as well as values of P_b for depths of 8, 12, 15, and 17 m. The blue dashed line indicates the approximation of the experimental data using equation (8), while the red line represents the approximation using equation (9)

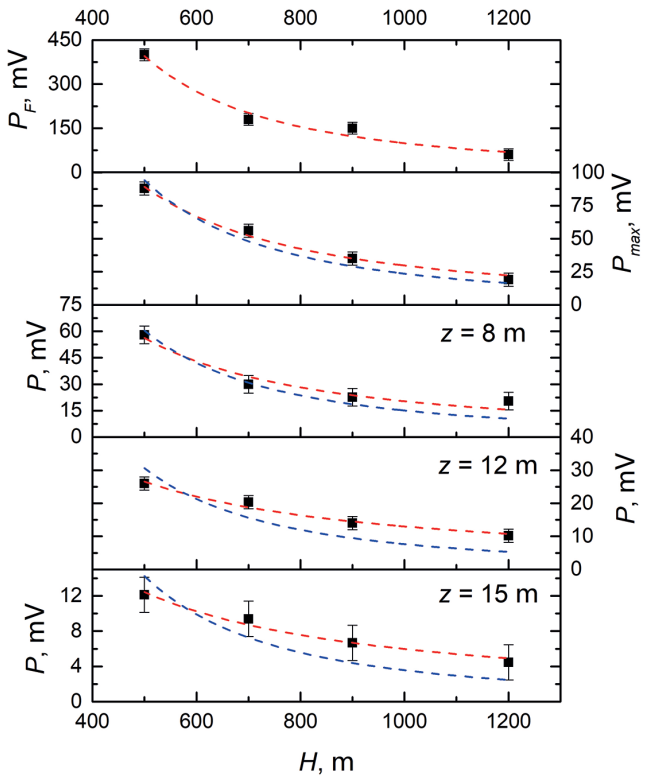

Fig. 4. Values of the echo signal amplitude for the case of the maximum from the upper water layers P_{max}, as well as values of P for depths of 8, 12, and 15 m. The blue dashed line indicates the approximation of the experimental data using equation (8), while the red line represents the approximation using equation (9)

Figure 5 shows the estimates of the magnitude of the function $f_3(z)$ as a function of the sounding depth, obtained for water layers using Eq. (13). The red dashed line represents the approximation of the obtained data using a function of the type given in (12), which includes a third-degree term in z.

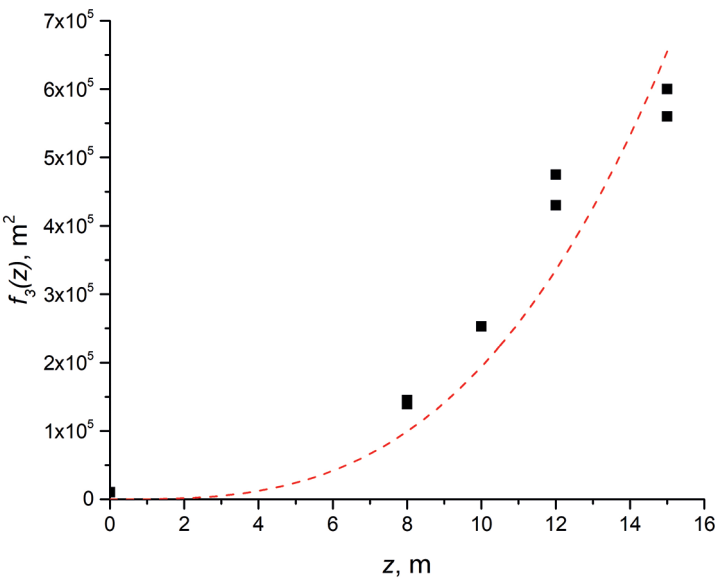

Fig 5. The assessment of the values of the function $f_3(z)$ as a function of sounding depth, obtained using equation (13)

To assess the contribution of the light intensity distribution variance $D(z)$ to the attenuation of the lidar echo signal, we consider the ratio of the values of the functions $f_3(z)$ and $f_2(H, z)$ for different sounding altitudes as a function of the bottom depth (Fig. 6). It is evident that as the sounding depth increases, the contribution of the function $D(z)$ becomes significant in comparison to the geometric factor.

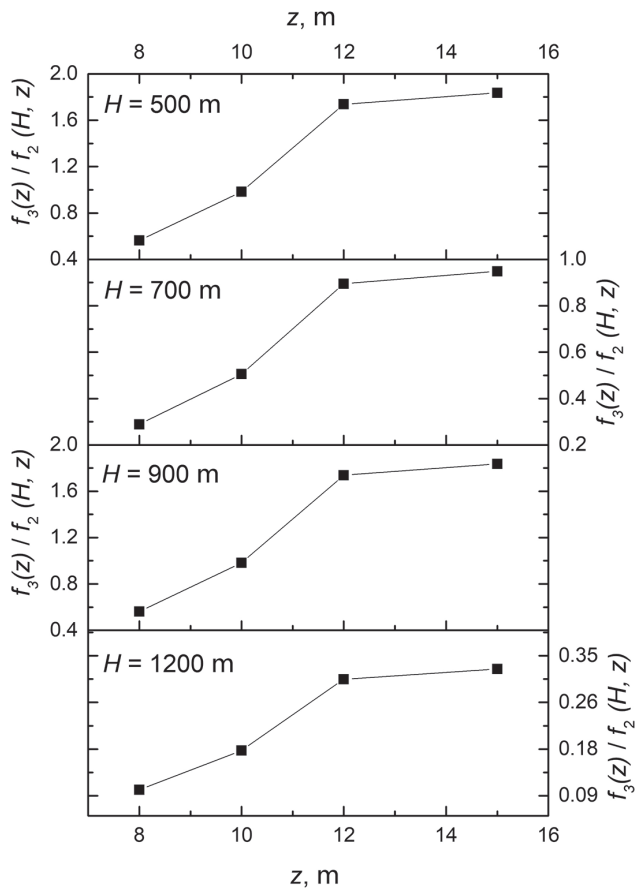

Fig. 6. The ratio of the $f_2(H, z)$ and $f_3(z)$ function values for different sounding altitudes as a function of depth z

The value of $f_3(z) \approx 0$ is obtained under the assumption that the echo signal is formed due to single scattering from a Lambertian surface located at a depth z, provided that the divergence of the sounding beam θ_1 is small and the field of view angle of the receiving system θ_2 is significantly larger than the divergence of the sounding beam (i. e., $\theta_1 << \theta_2$). In this case, the diameter of the illuminated area on the bottom D_b, lit by the sounding beam, equals the product of the length of the sounding path and the divergence of the sounding beam. This condition is satisfied by Fresnel reflection from the water surface, where the diameter of the illuminated area is determined solely by the divergence of the sounding beam and is sufficiently small. When the bottom is at a depth z_b, the contribution of multiple scattering along the path from the water surface to the bottom and back results in an increase in the area on the water surface D_s through which the radiation reflected from the bottom and entering the receiver emerges. With an increase in z_b, the contribution of multiple scattering also increases. The size of the area D_s becomes larger than the size of the area that falls within the field of view of the receiver D_r. As the sounding altitude increases, the ratio of the diameters of the areas D_r/D_s decreases, which leads to a reduction in the attenuation rate of the lidar echo signal and, consequently, an increase in the contribution of the function $D(z)$. Similar processes occur when reflecting off water layers located at fixed depths.

4. Conclusion

The results of field experiments demonstrated that the dependence of the magnitude and shape of the lidar echo signal on the length of the sounding path when investigating water layers and seabed exhibits a more complex behavior than what is predicted by the lidar Eq. (3) in its conventional form. This complexity is likely due to the contribution of multiple scattering along the path from the water surface to the sounding object and back, which causes the scattering of the laser spot at the depth of the sounded layer to not fully fall within the field

of view of the photodetector. In this case, the introduction of an additional term $D(z)$ into the lidar equation, which defines the dispersion of the illumination distribution in the cross-section of an infinitely narrow beam of light that has passed through a water layer of thickness z, allows for a more accurate description of the experimental dependencies obtained. Field experiments are complex and costly, thus Monte Carlo simulation would serve as an effective tool for verifying the accuracy of the employed form of the lidar equation. Future work in this area should focus on investigating the influence of the aforementioned effect in relation to the lengths of atmospheric and underwater sections in waters with varying hydrooptical characteristics.

Acknowledgments

The authors gratefully acknowledge M.L. Sbitnoy for organizing the flights over Bechevinskaya Bay and L.S. Dolin for useful recommendations used in conducting this work.

Funding

The research was carried out within the state assignment of Ministry of Science and Higher Education of the Russian Federation for the Shirshov Institute of Oceanology (IO RAS) (theme No. FMWE-2024-0028).

References

1. *Churnside J.H.* Review of profiling oceanographic lidar. *Optical Engineering*. 2014;53(5): 051405–051405. doi:10.1117/1.OE.53.5.051405
2. *Chen W., Chen P., Zhang H.* et al. Review of airborne oceanic lidar remote sensing. Intelligent Marine Technology Systems. 2023;1(10). doi:10.1007/s44295-023-00007-y
3. *Glukhov V.A., Goldin Yu.A.* Marine profiling lidars and their application for oceanological problems. *Fundamental and Applied Hydrophysics*. 2024;17(1):104–128. doi:10.59887/2073-6673.2024.17(1)-9
4. *Vasilkov A.P., Goldin Yu.A., Gureev B.A.* et al. Airborne polarized lidar detection of scattering layers in the ocean. *Applied Optics*. 2001;40(24):4353–4364. doi:10.1364/AO.40.004353
5. *Churnside J.H., Donaghay P.L.* Thin scattering layers observed by airborne lidar. *ICES Journal of Marine Science*. 2009;66(4):778–789. doi:10.1093/icesjms/fsp029
6. *Collister B.L., Zimmerman R.C., Hill V.J.* et al. Polarized lidar and ocean particles: insights from a mesoscale coccolithophore bloom. *Applied Optics*. 2020;59(15):4650–4662. doi:10.1364/AO.389845
7. *Peituo Xu, Dong Liu, Yibing Shen* et al. Design and validation of a shipborne multiple-field-of-view lidar for upper ocean remote sensing. *Journal of Quantitative Spectroscopy and Radiative Transfer*. 2020;254:107201. doi:10.1016/j.jqsrt.2020.107201
8. *Glukhov V.A., Goldin Yu.A., Glitko O.V.* et al. Investigation of the Relationships between the Parameters of Lidar Echo Signals and Hydrooptical Characteristics in the Western Kara Sea. *Oceanology*. 2023;63(S1): S119–S130. doi:10.1134/S0001437023070044
9. *Glukhov V.A., Goldin Yu.A., Glitko O.V., Glukhovets D.I., Rodionov M.A.* A comparison of the Information Content of Orthogonally Polarized Components of Lidar Echo Signal for Evaluating Hydrooptical Characteristics of the Near-Surface Layer. *Fundamental and Applied Hydrophysics*. 2024;17(3):32–43. doi:10.59887/2073–6673.2024.17(3)-3
10. *Churnside J.H., Marchbanks R.D., Le J.H.* et al. Airborne lidar detection and characterization of internal waves in a shallow fjord. *Journal of Applied Remote Sensing*. 2012;6(1):063611–063611. doi:10.1117/1.JRS.6.063611
11. *Dolin L.S., Dolina I.S., Savel'ev V.A.* A lidar method for determining internal wave characteristics. *Izvestiya, Atmospheric and Oceanic Physics*. 2012;48(4):444–453.
12. *Glukhov V.A., Goldin Yu.A., Rodionov M.A.* Method of Internal Waves Registration by Lidar Sounding in Case of Wa ters with Two-Layer Sratification of Hydrooptical Characteristics. *Fundamental and Applied Hydrophysics*. 2021;14(3):86–97. doi:10.7868/S2073667321030084 (in Russian).
13. *Philpot W.* Airborne Laser Hydrography II. 2019. doi:10.7298/JXM9-G971
14. Riegl VQ-880-G Data sheet. URL: http://www.riegl.com/uploads/tx_pxpriegldownloads/Infosheet_VQ-880-G_2016-05-23.pdf (Accessed: 21.02.2025).
15. *Lin Wu, Yifu Chen, Yuan Le* et al. A high-precision fusion bathymetry of multi-channel waveform curvature for bathymetric LiDAR systems. *International Journal of Applied Earth Observation and Geoinformation*. 2024;128(103770). doi:10.1016/j.jag.2024.103770
16. *Mandlburger G.* A review of active and passive optical methods in hydrography. *The International Hydrographic Review*. 2022;28:8–52. doi:10.58440/ihr-28-a15

17. *Mandlburger G., Hauer C., Wieser M., Pfeifer N.* Topo-Bathymetric LiDAR for Monitoring River Morphodynamics and Instream Habitats — A Case Study at the Pielach River. *Remote Sensing*. 2015;7:6160–6195. doi:10.3390/rs70506160
18. *Glukhov V.A., Goldin Yu.A., Rodionov M.A., Gureev B.A., Glitko O.V.* Airborne lidar bathymetry of coastal areas at night flight altitude. *Fundamental and Applied Hydrophysics*. 2019;12(4):85–93. (In Russian) doi:10.7868/S2073667319040105
19. *Churnside J. H., Hair J.W., Hostetler C.A., Scarino A.J.* Ocean backscatter profiling using high-spectral-resolution lidar and a perturbation retrieval. *Remote Sensing*. 2018;10(12):2003. doi:10.3390/rs10122003
20. *Lu X., Hu Y., Trepte C., Zeng S., Churnside J.H.* Ocean sub-surface studies with the CALIPSO spaceborne lidar. *Journal of. Geophysical Research. Oceans*. 2014;119:4305–4317. doi:10.1002/2014JC009970
21. *Kim M., Kopilevich, Y., Feygels V.* et al. Modeling of airborne bathymetric lidar waveforms. In: Brock, J.C.; Gesch, D.B.; Parrish, C.E.; Rogers, J.N., and Wright, C.W. (eds*.), Advances in Topobathymetric Mapping, Models, and Applications. Journal of Coastal Research, Special Issue*. 2016;76:18–30. Coconut Creek (Florida), ISSN0749–0208.
22. *Kim M.* Airborne Waveform Lidar Simulator Using the Radiative Transfer of a Laser Pulse. *Appl. Sci*. 2019;9(12):2452. doi:10.3390/app9122452
23. *Glukhov V.A., Goldin Yu.A., Glitko O.V., Rodionov M.A.* Airborne polarizing lidar for surveying marine areas. *Proceedings of the XXVIII International Symposium "Optics of the atmosphere and ocean. Atmospheric Physics"*, Tomsk, July 04–08, 2022. Tomsk, Publishing House of IOA SB RAS, 2022, 187–190 (in Russian).
24. *Glukhov V.A.* The patterns of backscatter signal formation in LIDAR sounding of the near-surface layers of seawater and the seafloor. *Diss. ... kand. fiz.-mat. nauk. M*., 2024. 115 p. (in Russian).
25. *Wang C. K., Philpot W.D.* Using airborne bathymetric lidar to detect bottom type variation in shallow waters. *Remote Sensing of Environment*. 2007;106(1):123–135. doi:10.1016/j.rse.2006.08.003
26. *Gordon H.R.* Interpretation of airborne oceanic lidar: effects of multiple scattering. *Applied Optics*. 1982;21(16):2996–3001. doi:10.1364/AO.21.002996
27. *Dolina I.S., Dolin L.S., Levin I.M., Rodionov A.A., Savel'ev V.A.* Inverse problems of lidar sensing of the ocean. *Current Research on Remote Sensing, Laser Probing, and Imagery in Natural Waters. SPIE*. 2007;6615:104–113.

Литература

1. *Churnside J.H.* Review of profiling oceanographic lidar // Optical Engineering. 2014. Vol. 53, No 5. P. 051405–051405. doi:10.1117/1.OE.53.5.051405 EDN: SOSNBF
2. *Chen W., Chen P., Zhang H.* et al. Review of airborne oceanic lidar remote sensing // Intelligent Marine Technology Systems. 2023. Vol. 1, N10. doi:10.1007/s44295-023-00007-y EDN: CKSHDC
3. *Глухов В.А., Гольдин Ю.А.* Морские радиометрические лидары и их использование для решения океанологических задач // Фундаментальная и прикладная гидрофизика. 2024. Т. 17, No 1. С. 104–128. doi:10.59887/2073-6673.2024.17(1)-9 EDN: YMUPXI
4. *Vasilkov A.P., Goldin Yu.A., Gureev B.A.* et al. Airborne polarized lidar detection of scattering layers in the ocean // Applied Optics. 2001. Vol. 40, N24. P. 4353–4364. doi:10.1364/AO.40.004353 EDN: LGLRSB
5. *Churnside J.H., Donaghay P.L.* Thin scattering layers observed by airborne lidar // ICES Journal of Marine Science. 2009. Vol. 66, No 4. P. 778–789. doi:10.1093/icesjms/fsp029 EDN: MYWKLP
6. *Collister B.L., Zimmerman R.C., Hill V.J.* et al. Polarized lidar and ocean particles: insights from a mesoscale coccolithophore bloom // Applied Optics. 2020. Vol. 59, No 15. P. 4650–4662. doi:10.1364/AO.389845 EDN: PWHSKU
7. *Peituo Xu, Dong Liu, Yibing Shen* et al. Design and validation of a shipborne multiple-field-of-view lidar for upper ocean remote sensing // Journal of Quantitative Spectroscopy and Radiative Transfer. 2020. Vol. 254. P. 107201. doi:10.1016/j.jqsrt.2020.107201 EDN: DZGWAC
8. *Glukhov V.A., Goldin Yu.A., Glitko O.V.* et al. Investigation of the Relationships between the Parameters of Lidar Echo Signals and Hydrooptical Characteristics in the Western Kara Sea // Oceanology. 2023. Vol. 63 (S1). P. S119–S130. doi:10.1134/S0001437023070044 EDN: ZXMTFQ
9. *Глухов В.А., Гольдин Ю.А., Глитко О.В., Глуховец Д.И., Родионов М.А.* Сопоставление информативности ортогонально поляризованных компонент лидарного эхо-сигнала для оценки гидрооптических характеристик приповерхностного слоя // Фундаментальная и прикладная гидрофизика. 2024. Т. 17. No. 3. С. 32–43. doi:10.59887/2073-6673.2024.17(3)-3 EDN: DEOVKB
10. *Churnside J.H., Marchbanks R.D., Le J.H.* et al. Airborne lidar detection and characterization of internal waves in a shallow fjord // Journal of Applied Remote Sensing. 2012. Vol. 6, No 1. P. 063611–063611. doi:10.1117/1.JRS.6.063611 EDN: UTDAVV
11. *Долин Л.С., Долина И.С., Савельев В.А.* Лидарный метод определения характеристик внутренних волн // Известия РАН. Физика атмосферы и океана. 2012. Т. 48, № 4. С. 501–501. EDN: PANHOZ

12. *Глухов В.А., Гольдин Ю.А., Родионов М.А.* Лидарный метод регистрации внутренних волн в водах с двухслойной стратификацией гидрооптических характеристик // Фундаментальная и прикладная гидрофизика. 2021. Т. 14, No 3. С. 86–97. doi:10.7868/S2073667321030084 EDN: FZLYDG
13. *Philpot W.* Airborne Laser Hydrography II. 2019. doi:10.7298/JXM9-G971
14. Riegl VQ-880-G Data sheet [Электронный ресурс]. URL: http://www.riegl.com/uploads/tx_pxpriegldownloads/Infosheet_VQ-880-G_2016-05-23.pdf (дата обращения: 21.02.2025).
15. *Lin Wu, Yifu Chen, Yuan Le* et al. A high-precision fusion bathymetry of multi-channel waveform curvature for bathymetric LiDAR systems // International Journal of Applied Earth Observation and Geoinformation. 2024. Vol. 128, No. 103770. doi:10.1016/j.jag.2024.103770 EDN: GPBYXD
16. *Mandlburger G.* A review of active and passive optical methods in hydrography // The International Hydrographic Review. 2022. No. 28. P. 8–52. doi:10.58440/ihr-28-a15 EDN: AOUMWW
17. *Mandlburger G., Hauer C., Wieser M., Pfeifer N.* Topo-Bathymetric LiDAR for Monitoring River Morphodynamics and Instream Habitats — A Case Study at the Pielach River // Remote Sensing. 2015. Vol. 7. P. 6160–6195. doi:10.3390/rs70506160
18. *Глухов В.А., Гольдин Ю.А., Родионов М.А., Гуреев Б.А., Глитко О.В.* Авиационная лидарная батиметрическая съемка прибрежных акваторий с большой высоты // Фундаментальная и прикладная гидрофизика. 2019. Т. 12, No. 4. С. 85–93. doi:10.7868/S2073667319040105 EDN: ZCARMN
19. *Churnside J. H., Hair J.W., Hostetler C.A., Scarino A.J.* Ocean backscatter profiling using high-spectral-resolution lidar and a perturbation retrieval // Remote Sensing. 2018. Vol. 10, No. 12. P. 2003. doi:10.3390/rs10122003 EDN: YXVEZQ
20. *Lu X., Hu Y., Trepte C., Zeng S., Churnside J.H.* Ocean sub-surface studies with the CALIPSO spaceborne lidar // J. Geophys. Res. Oceans. 2014. Vol. 119. P. 4305–4317. doi:10.1002/2014JC009970 EDN: UVNTSD
21. *Kim M., Kopilevich Y., Feygels V.* et al. Modeling of airborne bathymetric lidar waveforms // Advances in Topobathymetric Mapping, Models, and Applications. Journal of Coastal Research, Special Issue. 2016. No. 76. P. 18–30. doi:10.2112/SI76-003 EDN: YUWOGX
22. *Kim M.* Airborne Waveform Lidar Simulator Using the Radiative Transfer of a Laser Pulse // Appl. Sci. 2019. Vol. 9, No. 12. P. 2452. doi:10.3390/app9122452 EDN: JRTWOA
23. *Глухов В.А., Гольдин Ю.А., Глитко О.В., Родионов М.А.* Авиационный поляризационный лидар для съемки морских акваторий // Труды XXVIII Международного симпозиума «Оптика атмосферы и океана. Физика атмосферы», г. Томск, 04–08 июля 2022 г. Томск: Издательство ИОА СО РАН, 2022. С. 187–190. EDN: OOMJPU
24. *Глухов В.А.* Закономерности формирования сигналов обратного рассеяния при лидарном зондировании приповерхностных слоев морской воды и дна: дис. ... канд. физ.-мат. наук. М., 2024. 115 с.
25. *Wang C. K., Philpot W.D.* Using airborne bathymetric lidar to detect bottom type variation in shallow waters // Remote sensing of Environment. 2007. Vol. 106, № . 1. P. 123–135. doi:10.1016/j.rse.2006.08.003 EDN: LWZDYT
26. *Gordon H.R.* Interpretation of airborne oceanic lidar: effects of multiple scattering // Applied Optics. 1982. Vol. 21, No 16. P. 2996–3001. doi: 10.1364/AO.21.002996
27. *Dolina I.S., Dolin L.S., Levin I.M., Rodionov A.A., Savel'ev V.A.* Inverse problems of lidar sensing of the ocean // Current Research on Remote Sensing, Laser Probing, and Imagery in Natural Waters. SPIE. 2007. Vol. 6615. P. 104–113.

About the Authors

VLADIMIR A. GLUKHOV, Researcher, St. Petersburg Branch of IO RAS, Cand.Sc. (Phys.-Math.), ORCID: 0000-0003-4555-8879, WoS ResearcherID: GSD-4886–2022, Scopus AuthorID: 57191414331, SPIN-code (РИНЦ): 9449-2307, e-mail: vl.glukhov@inbox.ru

YURY A. GOLDIN, Leading Researcher, IO RAS, Cand.Sc. (Phys.-Math.), ORCID: 0000-0001-5731-5458, Scopus Author ID: 6602648464, SPIN-code (РИНЦ): 2750-1867, e-mail: goldin@ocean.ru

OLEG V. GLITKO, Researcher, St. Petersburg Branch of IO RAS, ORCID: 0009-0005-2313-2326. e-mail: glitko_kisin@mail.ru